Models to analyze small-angle neutron scattering from unilamellar lipid vesicles

Norbert Kučerka* and John F. Nagle†
Physics Department, Carnegie Mellon University, 5000 Forbes Avenue, Pittsburgh, Pennsylvania 15213, USA

Scott E. Feller‡
Department of Chemistry, Wabash College, Crawfordsville, Indiana 47933, USA

Pavol Balgavý§
Department of Physical Chemistry of Drugs, Faculty of Pharmacy, Comenius University, Odbojárov 10, 832 32 Bratislava, Slovakia
(Received 8 December 2003; published 6 May 2004)

Small-angle scattering has been employed to study the structure of lipid bilayers in unilamellar vesicles. This paper evaluates the use of a model approach for the analysis of such data. A long molecular dynamics simulation of a dipalmitoylphosphatidylcholine bilayer in the L_α phase provides detailed structural information from which scattering length density profiles and scattering intensity are obtained. A sequence of increasingly realistic models are defined and then fit to the simulated scattering intensity data for values of q that are experimentally accessible. The models are evaluated by how well they fit the intensity data and the structural parameters of the simulation. Although the conventional approach that extracts only the radius of gyration from a Kratky-Porod plot provides a reasonable fit to much of the data, the available experimental q range supports refined models with two independent parameters. Of the many two-parameter models, we propose that particular choices should be inspired by the functional form of the scattering length density profile of simulations. Constraints that limit realistic models to two independent parameters are described in detail. The analysis supports the proposition that reliable results for area/lipid and hydrocarbon thickness can be obtained from small-angle neutron scattering of unilamellar vesicles.

DOI: 10.1103/PhysRevE.69.051903 PACS number(s): 87.16.Dg, 87.64.Bx, 61.12.Ex

I. INTRODUCTION

One of the most important parameters that describes the lipid bilayers that underlie the structure of biomembranes is the bilayer thickness; this structural property is one that affects the properties of intrinsic membrane proteins. Another central structural parameter is the average area A occupied by a lipid along the surface of the bilayer. There have been two approaches to obtaining such structural parameters using x-ray and neutron methods. The first approach studies samples composed of multibilayer arrays, either multilamellar vesicles or oriented stacks of bilayers, to construct electron density profiles from the intensities of the diffraction peaks. For the biologically most relevant fluid (L_α) phase the method of obtaining the electron density profiles following the usual crystallographic methodology breaks down when the sample is fully hydrated [1] because the higher order diffraction peaks are corrupted by the loss of intensity into diffuse scattering. A new development uses the diffuse scattering as a continuous function of the scattering vector q instead of the diffraction peaks to obtain the electron density profile as well as the elastic moduli (bending modulus and compressibility modulus) for the liquid crystal array [2].

The second approach to lipid bilayer structure that is the subject of this paper studies samples composed of unilamellar vesicles instead of multilamellar arrays. Unilamellar vesicles are attractive because they are topologically equivalent to cells with an interior and an exterior. As such, they should have advantages in future studies of peptides or other additives in membranes [3,4]. Of course, instead of having strong discrete diffraction peaks that occur for multilamellar arrays, the scattering of x rays or neutrons from unilamellar vesicles is continuous in the scattering vector q, which is advantageous because more data are obtained. The disadvantage is that the scattering intensities are weaker and so the weaker scattering at higher q is undetectable. In a pioneering x-ray study [5], the intensities could only be observed up to about $q=0.3$ Å^{-1}; maximum q values for multilamellar arrays are twice as large [2]. Experimentally obtained data indicate that neutron scattering can be detected up to about $q=0.2$ Å^{-1} [6].

Most analysis of neutron scattering from unilamellar vesicles has been performed by fitting the scattering data to a simple single-strip model where the scattering length density across the bilayer is constant [6–14]. However this single-strip model neglects the inner structure of the bilayer. At a minimum, the bilayer consists of three strips, one for the hydrocarbon region and two for the polar headgroups, and it is well known that there is water inside the polar headgroup regions. Molecular dynamics simulations also show additional substructure within the bilayer [15–17].

Therefore, in this paper we have developed more realistic models of bilayers to use for analyzing neutron-scattering

*Also at Department of Chemical Theory of Drugs, Faculty of Pharmacy, Comenius University, Kalinčiakova 8, 832 32 Bratislava, Slovakia. Electronic address: kucerka@andrew.cmu.edu
†Electronic address: nagle@andrew.cmu.edu
‡Electronic address: fellers@wabash.edu
§Electronic address: pavol.balgavy@fpharm.uniba.sk

data. The simplest logical extension would just add more strips to the model. However, instead of blindly following that procedure, we believe that molecular dynamics simulations provide reliable information about the functional form of the scattering length profile that can guide the design of better models. This use of simulations does not rely on numerical results obtained by simulations for bilayer thickness or other structural parameters; such simulation results are dependent on the area per molecule A chosen for fixed A simulations [18] or upon finite size effects [19] or the chosen surface pressure when a constant surface pressure ensemble is used [20,21]. However, the functional form of the scattering length profile does not change significantly even when the structural parameters vary significantly. Therefore, our program is to obtain the best values of the structural parameters by fitting a good functional form, inspired by simulations, to neutron-scattering data.

The first aim in this paper is to develop appropriate models and to obtain the quantitative scattering intensity for these models. The scattering intensity formulas are not as simple as for the single-strip model, but the computational effort in fitting the models to data is still quite modest. The second aim is to evaluate whether current neutron-scattering data are extensive enough to evaluate the parameters in the models and, in particular, to estimate how complex the model can be before the data are no longer capable of providing well determined values for the parameters. To achieve these aims we use simulations for the benchmark dipalmitoylphosphatidylcholine (DPPC) bilayer to provide a well-defined test case, as well as to refine our models.

In Sec. II the results of a simulation are combined with the theory of small-angle neutron scattering from unilamellar vesicles to produce a well-defined test case. Section III introduces a sequence of increasingly realistic models. The calculated scattering intensity of each of these models is fit to the test case scattering intensity, thereby determining the physical parameters in the model. The models are evaluated by how well they can fit the scattering data and by how well the physical parameters describe the structure determined by the simulation. Section IV compares the models and it also compares to more conventional methods based on Kratky-Porod plots and the Guinier approximation.

II. SCATTERING PREDICTED BY SIMULATIONS

The molecular dynamics simulation system consists of 72 DPPC molecules at full hydration (29.1 waters/lipid) with a fixed average surface area $A_L = 62.9\ Å^2$ per lipid molecule, a constant normal pressure of 1 atm, and a constant temperature of 50°C. The CHARMM program [22] was employed using the potential energy parameters described in Ref. [23]. A time step of 2 fs was employed with conformations saved every picosecond during the 10 ns simulation.

We will use the volume probability distribution functions for the molecular components of the dipalmitoylphosphatidylcholine (DPPC) molecule in bilayers [18,24]. The six component groups of DPPC consist of (1) the terminal methyls (CH_3) on the hydrocarbon chains, (2) the methylenes (CH_2) on the hydrocarbon chains, (3) the carbonyls (C═O)

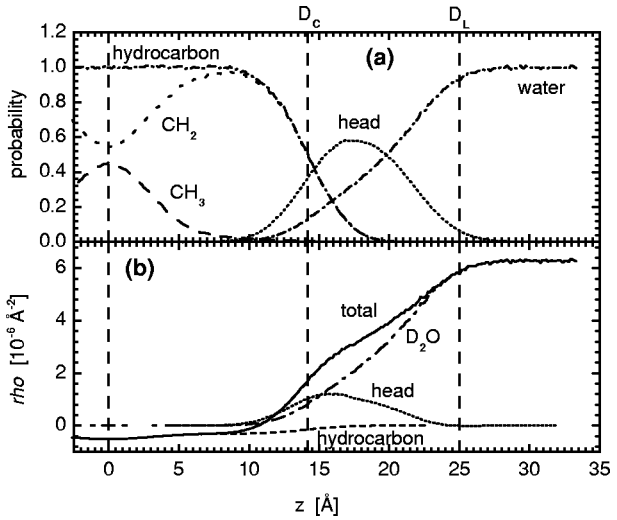

FIG. 1. (a) Probability (volume fractions) distributions for water, polar headgroups, and total hydrocarbon chains (including the breakdown into methylenes and terminal methyls) as functions of z along the bilayer normal. The DPPC bilayer with $A = 62.9\ Å^2$ is symmetrically centered at $z = 0$. The Gibbs dividing surface for the hydrocarbon chain region is shown as D_C and the monolayer steric thickness is shown as D_L. (b) shows the total calculated neutron-scattering length density (solid line) for (a) in heavy water, as well as the individual contributions from hydrocarbon, polar heads, and D_2O.

where the chains join the (4) glycerol ($C_3O_2H_5$) backbone, (5) the phosphate (PO_4) part of the headgroup and (6) the choline [$(CH_2)_2N(CH_3)_3$] part of the headgroup. For clarity Fig. 1(a) only shows the composite headgroup probability distribution which consists of the sum of components 3–6, as well as deuterated water which may be considered component (7). From this figure we can obtain another important physical parameter that will be used to test our models, namely, the location $D_C = 14.2$ Å of the Gibbs dividing surface between the hydrocarbon region and the polar headgroup region [1]. From the known scattering length density of the atoms in each of the seven component groups, we calculated the profile of the neutron-scattering length density $\rho(z)$ along the normal z of the bilayer in heavy water as is shown in Fig. 1(b).

Generally for a system of unilamellar vesicles all of the same size the experimentally observed coherent scattering intensity is given by

$$I(q) = N|F(q)|^2 S(q), \tag{1}$$

where the scattering vector $q = (4\pi/\lambda)\sin(\vartheta/2)$, N is the number of vesicles, $F(q)$ is the form factor of one vesicle, and $S(q)$ is the intervesicle structure factor. The form factor $F(q)$ is the Fourier transform of the contrast $\Delta\rho(r)$ between coherent neutron-scattering length density of the vesicular bilayer and the solvent. For a vesicle that is isotropic and statistically centrosymmetric

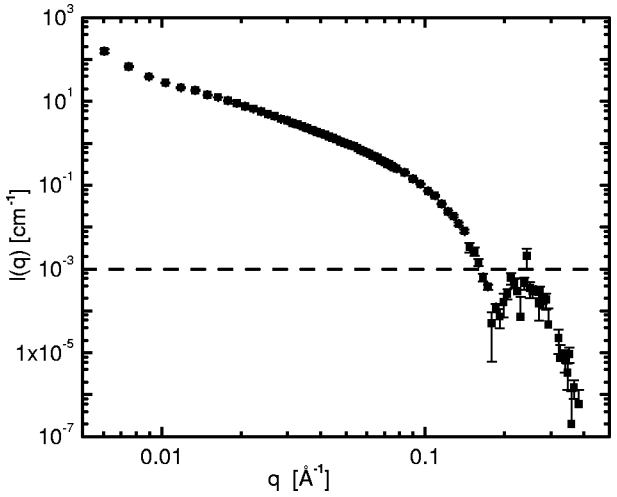

FIG. 2. Scattering curve $I(q)$ constructed from $\rho(z)$ in Fig. 1. Error bars are comparable to experiment [26,32]. The horizontal dashed line shows the level of the instrumental cutoff for protonated DPPC in D_2O.

$$F(q) = (4\pi/q)\int_{R_{in}}^{R_{out}} \Delta\rho(r)\sin(qr)r\ dr, \qquad (2)$$

where R_{in}, R_{out} are inner and outer radii, respectively, outside of which $\Delta\rho(r)=0$. The average outer radius R_{out} of the vesicles studied experimentally is about 300 *Å* [25–27]. The Debye approximation of the interparticle structure factor $S(q)$ for spherical vesicles [28,29], which assumes nonspecific association (just steric avoidance) of vesicles, then predicts that $S(q)$ is very nearly unity for $q>0.01$ Å^{-1}. Experimentally, for *p*H neutral aqueous dispersions of uncharged unilamellar vesicles with total phospholipid concentrations less than 2 wt. %, $S(q)$ is close to unity even for $q>0.005$ Å^{-1} [12,30].

The predicted scattering intensity was calculated for monodisperse unilamellar spherical vesicles employing the scattering length density $\rho(z)$ from the simulation and Eqs. (1) and (2). Polydispersity was then included by convolution with a Schulz distribution $G(R)$ [31] of spheres with a mean radius $R_{out}=300$ Å and a size polydispersity $\sigma_R \sim 90$ Å, typical of extruded vesicles in experiments [25–27]. As was emphasized there and as can be seen in Fig. 2, polydispersity dampens the rapid $\pi h/R$ vesicle oscillations that would occur for monodisperse vesicles. Only the $h=1$ minimum is noticeable near $q=0.01$ Å^{-1} in Fig. 2. It is only in this very small-angle region that the scattering is sensitive to the precise values of the vesicle size distribution and it is from these data that values of the vesicle radius and vesicle polydispersity were obtained [25,27]. However, in this paper we focus on the region $q>0.02$ Å^{-1}. In this region the intensity is insensitive to the precise values of R and σ_R or to deviations from sphericality due to undulation fluctuations and it is much more sensitive to the local structure of the bilayer, which is the subject of most interest.

We have added simulated noise to the $I(q)$ result shown in Fig. 2 with the same relative uncertainties as experimental data [26,32]. We have also added the resolution function of the spectrometer; this impacts the measured scattering curve mainly in the region of high values of scattering vector, where it smears intrinsic values of scattering intensity [27]. We simulate it by convolution of the theoretical function with a Gaussian distribution of q values around each particular value. For the values of the dispersion $\Delta q/q$ as well as for experimental errors we used our experimental values from the small-angle time-of-flight axially symmetric neutron-scattering spectrometer YuMO at the IBR-2 fast pulsed reactor of the Frank Laboratory of Neutron Physics, Joint Institute for Nuclear Research in Dubna [33–35].

Detection of neutron scattering becomes more difficult as q increases due to instrumental background and incoherent scattering. For protonated vesicles in D_2O the horizontal dashed line in Fig. 2 indicates the limitation of observable intensity, which is comparable in several studies [6,11,36]. Comparison to the calculation indicates that only upper bounds on the scattering intensity can be obtained for a DPPC sample for $q>0.17$ Å^{-1}.

It may also be noted that the incoherent scattering level increases as heavy water is replaced by light water; deuterating parts or all of the lipid reduces the incoherent background, but this also reduces the scattering intensity. Such contrast variation also dramatically changes the functional form of the scattering length density, so this paper concentrates on protonated lipid in D_2O.

III. MODELS

A. Single-strip 1S model

The neutron-scattering length density profile in this model consists of one homogenous strip as shown in Fig. 3, where the scattering length density contrast $\Delta\rho=\rho-\rho_W$ is taken constant through the bilayer. The model scattering curve was calculated using Eqs. (1) and (2). The radii R_i that are required for the form factor of the spherical vesicle are related to the z coordinate by $R_i=R-D_L+z_i$, where $2D_L$ is the total width of the single strip, which is therefore the parameter for the bilayer thickness in this model.

For this and all subsequent models we used the following method to compare a model with the molecular dynamics (MD) simulation. The bilayer parameters in a model (consisting of just D_L for the 1S model) are varied to minimize the difference between the model scattering curve and the scattering curve produced by the MD simulation in Fig. 2; the errors estimated from experiments were used to obtain the χ^2 estimation. For the 1S model the result is shown by the continuous curve in Fig. 3(c) and the model scattering density profile that produces this fit is shown in Fig. 3(a). The scattering intensity for the 1S model is plotted up to $q=0.4$ Å^{-1}; this shows that the 1S model predicts scattering intensity that would be observable above the instrumental cutoff for a q range near 0.25 Å^{-1}. One of us (N.K.) has taken considerable higher q data (unpublished) that confirms the absence of experimental scattering above this level [37]. This is strong evidence that the 1S model is inadequate.

Figure 3(a) shows that the 1S model is a rather primitive representation of the scattering length density of the DPPC

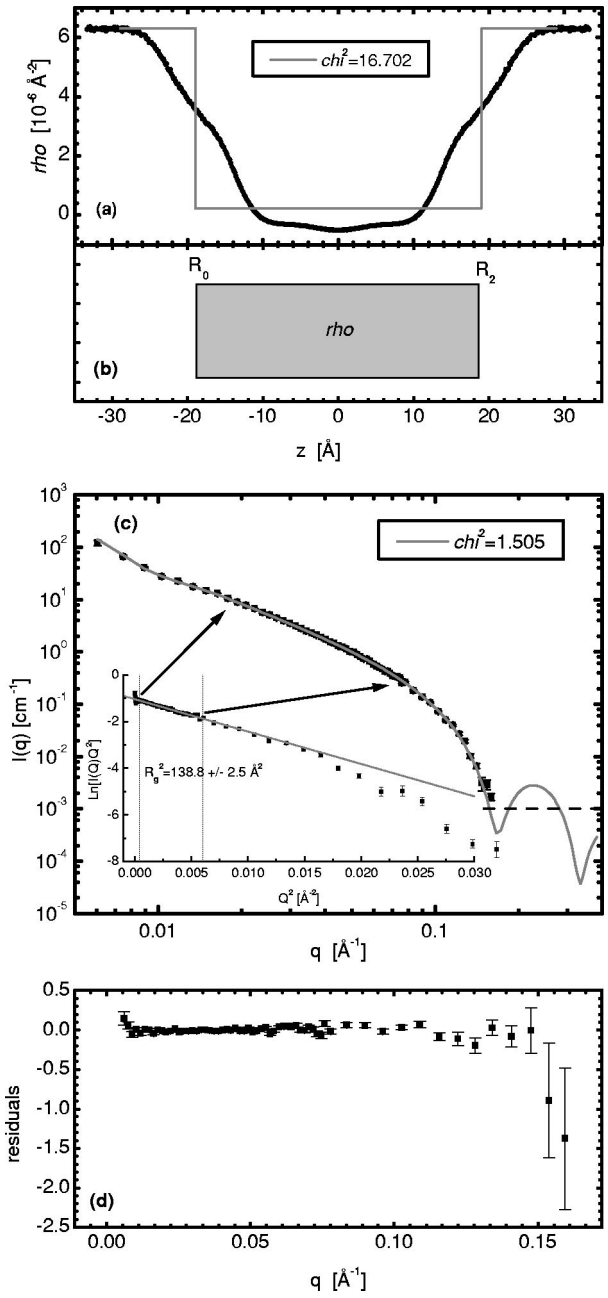

FIG. 3. Single-strip 1S model. (a) Circles show the MD neutron-scattering length density profile. The gray step function shows the values of the model parameters that best fits the scattering curve in (c). (b) Schematic of the single-strip model. (c) Solid squares show the MD scattering intensity from Fig. 2 and the solid gray line shows the best fit of the model. The inset shows the Kratky-Porod plot to the q region indicated by arrows. (d) shows the residuals to the fit.

bilayer. Nevertheless, the good fit that it provides to the scattering data in the observable range has made it a popular model [7,10,11,13]. Figure 3(d) shows the residuals to the fit in Fig. 3(c). Although Fig. 3(c) confirms the general consensus that the scattering data are quite well fit with a one-parameter 1S model, the systematic trend in the residuals in Fig. 3(d) and the prediction of intensity greater than the instrumental cutoff for $q > 0.2$ Å^{-1} indicates that the data support consideration of models with two independent parameters.

TABLE I. Physical parameters obtained by fitting models to simulated scattering compared to those obtained directly from the MD simulation. The hydrocarbon half thickness D_C and the steric half-thickness D_L are shown in Fig. 1, the polar thickness $D_P = D_L - D_C$. A_L is area/lipid and n'_W is number of water molecules in the polar region.

Model	n'_W	A_L (Å^2)	D_P (Å)	D_C (Å)	D_L (Å)	χ^2
MD	~11.9	62.9	~10.8	14.2	~25	
1S	0*	64.1			19.0	1.505
3S	7.6	61.8	9.0	14.4	23.4	1.034
3L	15.4	61.4	12.9	14.5	27.4	1.036
3T	11.4	62.0	10.8	14.4	25.2	1.035

It is also useful to place the classical Kratky-Porod (KP) plot in the perspective of the single-strip 1S model. The inset to Fig. 3(c) shows the KP plot from which one obtains only one structural parameter, the radius of gyration R_g, which is usually interpreted in terms of the bilayer thickness $2D_L$ of a single-strip model using $R_g^2 = D_L^2/3$ [26]. We further emphasize that the KP plot does not use the experimental data for the higher q values shown in Fig. 3(c). Pencer and Hallett [6] have proposed extracting a different single parameter from scattering data, namely, q_{PH} at which the plot of Iq^4 vs q is maximal; they estimate the bilayer thickness by $2D_L = \pi/q_{PH}$.

The 1S model does have a second parameter, namely, the constant $\Delta\rho$. Let us define B_L and V_L to be the neutron-scattering length and volume of the lipid molecule, B_W and V_W to be the corresponding quantities for the water molecule, and ρ_W is the neutron-scattering length density of the aqueous solvent. The only molecular organization that can be modeled by the 1S model consists of a homogeneous mixture of lipid and n'_W water molecules in the single strip, which would then require

$$\Delta\rho = \frac{B_L + n'_W B_W}{V_L + n'_W V_W} - \rho_W. \tag{3}$$

If the scattering intensity is carefully normalized to the sample concentration, then $\Delta\rho$ could be determined from the fit to the data and Eq. (3) would enable determination of n'_W. However, experimental scattering intensity is often determined only up to a scaling factor that depends on sample concentration represented by the number of vesicles N in Eq. (1). Indeed, the models to be developed in the following sections do not require or benefit from having the absolute scaling factor and the artificiality of the water distribution in this model does not warrant making that effort. Therefore, we prefer to characterize the 1S model as a one-parameter model, with the thickness D_L as the single parameter.

The 1S row in Table I gives the value of D_L from the fit in Fig. 3(c). If we assume that there is no water in the bilayer ($n'_W = 0$), then the area A_L is obtained as V_L/D_L where the lipid volume V_L in the simulation was 1215.5 Å^3.

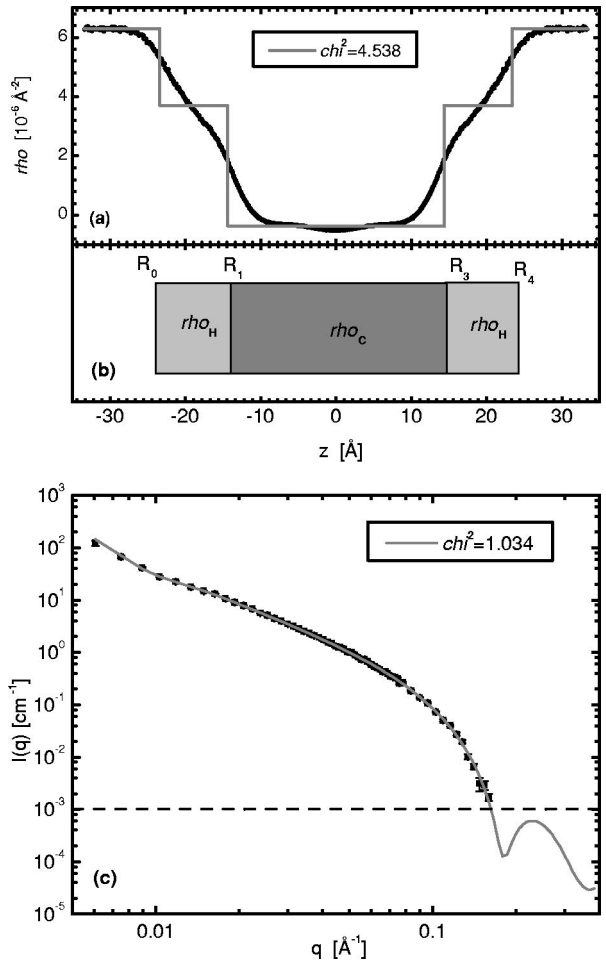

FIG. 4. Three-strip 3S model. (a) Neutron-scattering length density profile and (b) schematic of the model. See caption to Fig. 3 for description of fitted lines to the MD scattering density profile (a) and scattering curve (c).

B. Three-strip 3S model

Conventional model refinement adds more strips to the strip model [25,26,32]. For M strips the corresponding form factor is given by

$$F(q) = 4\pi \sum_{i=1}^{M} \int_{R_{i-1}}^{R_i} \Delta\rho_i \frac{\sin(qr)}{qr} r^2 dr$$

$$= \frac{4\pi}{q^3} \sum_{i=1}^{M} \Delta\rho_i [A(R_i) - A(R_{i-1})],$$

$$A(R_i) = qR_i \cos(qR_i) - \sin(qR_i). \tag{4}$$

In this section we add two more strips to the model as shown in Fig. 4(a). The form factor for this model was calculated using Eq. (4) with $M=3$.

At first sight, it would appear that the 3S model shown in Fig. 4(a) has at least three parameters, two lengths and one scattering length ratio, but there is a constraint that reduces the free parameters to two as we now show. We define the known scattering lengths to be B_C for the hydrocarbon chains, B_H for each of the headgroup, and B_W for each water molecule. Corresponding subscripts are used for the volumes V, which are also known to sufficient accuracy from the molecular dynamics simulation [24]. Then, similar to Eq. (3), the scattering length density in the headgroup region is

$$\Delta\rho_H = \frac{B_H + n'_W B_W}{V_H + n'_W V_W} - \rho_W, \tag{5}$$

where all the n'_W water molecules inside the bilayer are required to be homogeneously dispersed only in the polar headgroup region. Unlike the single-strip model, the scattering length density in the hydrocarbon region is determined by known quantities,

$$\Delta\rho_C = \frac{B_C}{V_C} - \rho_W, \tag{6}$$

where $V_C = V_L - V_H = 891.9$ Å^3. This means that the fitting provides the scaling factor for the scattering intensity normalized to amount of lipid, which therefore does not have to be carefully measured. Evaluation of n'_W in Eq. (5) is equivalent to evaluation of the ratio $\Delta\rho_C/\Delta\rho_H$.

Next, consider the following relation, involving the area per lipid A_L, the length D_P of the polar region, and the length D_C of the hydrocarbon chain region

$$A_L = \frac{V_H + n'_W V_W}{D_P} = \frac{V_C}{D_C}. \tag{7}$$

When analyzing real neutron-scattering data, one would use the headgroup volume $V_H = 325 \pm 6$ Å^3 that has been obtained from x-ray studies [38]. In this paper, where the neutron-scattering data are obtained from a simulation, we use $V_H = 323.5$ Å^3 that was obtained in the simulation [24]. Likewise, the chain volume $V_C = V_L - V_H$ would then be obtained from the lipid volume, determined experimentally as $V_L = 1232 \pm 2$ Å^3 [1], and $V_L = 1215.5$ Å^3 from the simulation. Equation (7) provides a constraint between the three model parameters D_P, D_C, and $\Delta\rho_C/\Delta\rho_H$ reducing the fit to two independent parameters.

The result of fitting this constrained 3S model to the MD simulated scattering data is shown in Fig. 4. The residuals of the fit (not shown) have no systematic deviation when compared to the noise level expected in experimental data. Perhaps even more important, the model does not predict larger intensity for $q > 0.2$ Å^{-1} than the instrumental cutoff intensity. This confirms that neutron-scattering data from unilamellar vesicles require models with at most two independent parameters. It might then be concluded that it is unnecessary to consider further refinements to the models, but we argue that this would be a shortsighted conclusion. The comparison of the scattering length density profile in Fig. 4(a) is certainly rather poor. Importantly, the values of the parameters D_P, D_C, n'_W, and A_L that emerge from such a fit may not be accurate measures of the molecular organization of the bilayer; we will return to this issue in Sec. IV after we consider refinements that better model the simulated scattering length

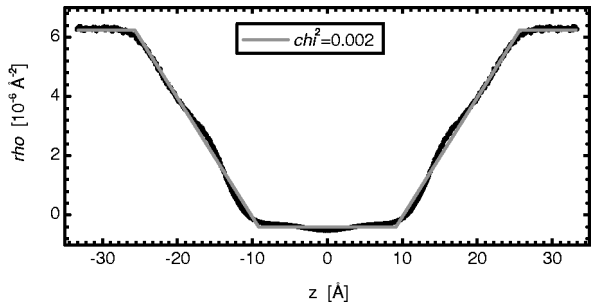

FIG. 5. Unconstrained 3L model: Neutron-scattering length density profile with nonconstrained linear course of density in the polar part.

density profile. Table I gives the values of the bilayer parameters from the fit in Fig. 4, where A_L was obtained using Eq. (7).

Let us briefly discuss refinement of strip models by adding more strips. The electron density profile for x-ray scattering (also the scattering length density profile for neutron scattering of a deuterated lipid bilayer) has a substantial minimum in the middle of the bilayer due to the terminal methyl groups on the hydrocarbon chains; this is especially pronounced in gel phases [38]. Therefore, for x-ray scattering the next feature that is added to strip models is a strip for the methyl trough. Figure 1(b) shows that such a trough is clearly a minor feature for neutron scattering for which the next strips that should be added would be an additional strip in each headgroup region. However, it is also clear that adding additional strips to approximate a nearly linear profile in the headgroup region is not only not very efficient, but would proliferate meaningless parameters. We therefore turn to models that are inspired by the molecular dynamics simulations.

C. Linear 3L model

The aim of this model is to improve the representation of the polar region. The MD simulation in Fig. 1 indicates that the scattering length density increases roughly linearly as z increases within the polar region, so we consider a linear scattering length density instead of a constant strip,

$$\Delta\rho = k_1^a r + k_2^a - \rho_W, \tag{8}$$

with fitting parameters k_1^a and k_2^a. This model fits the scattering length density well, as shown in Fig. 5. (Of course, it fits the simulated scattering intensity extremely well.) The obvious parameters in this model consist of two lengths. Unfortunately, because of the overlap of polar headgroups and hydrocarbon, the inner length of 10 Å shown in Fig. 5 is much smaller than the thickness D_C of the hydrocarbon region, which is defined to be the Gibbs dividing surface for the interface between the hydrocarbon region and the polar region in Fig. 1. There is therefore also no clear way to obtain area A_L using this model.

Our attempt to make this linear model more physical is shown in Fig. 6(a). Just as for the 3S model, there are two independent parameters when the constraint contained in Eq.

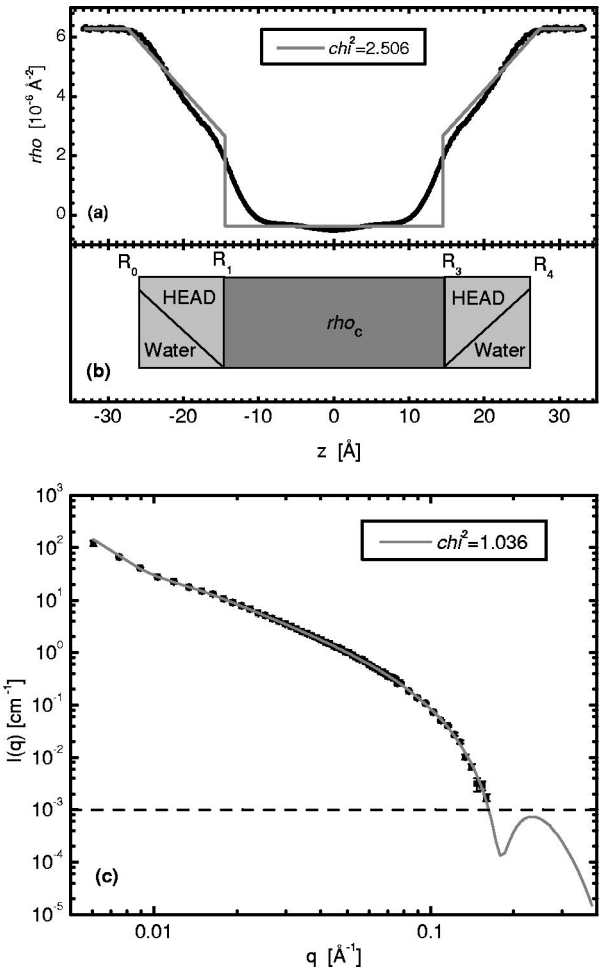

FIG. 6. Constrained 3L model: (a) Neutron-scattering length density profile and (b) schematic of the model. See caption to Fig. 3 for description of fitted lines to the MD scattering density profile (a) and scattering curve (c).

(7) is applied. The result from fitting the scattering curve in Fig. 6(c) is good enough for available neutron-scattering data (residuals not shown). The results for the physical parameters obtained for this model are shown in Table I. Comparison to the simulation is somewhat poorer than for the 3S model. Comparison of the scattering length density profiles in Fig. 6(a) suggests that this model may be further improved near the hydrocarbon/polar interface.

D. Triangular 3T model

In this model the volume fractions of water and hydrocarbon in the headgroup region shown in Fig. 1(a) are modeled as linear functions, as indicated in Fig. 7(b), and the triangular shape of headgroup itself accounts for the remainder of the polar volume. The assumptions in Fig. 7(b) are (1) that the volume of water in the headgroup region is twice as large as the volume of the hydrocarbon region and (2) that the hydrocarbon region only extends half way into the headgroup region. The linearity and these assumptions are approximations to the probability distributions shown in Fig. 1. Note that the distance $R_4 - R_2$ in Fig. 7(b) does not give the

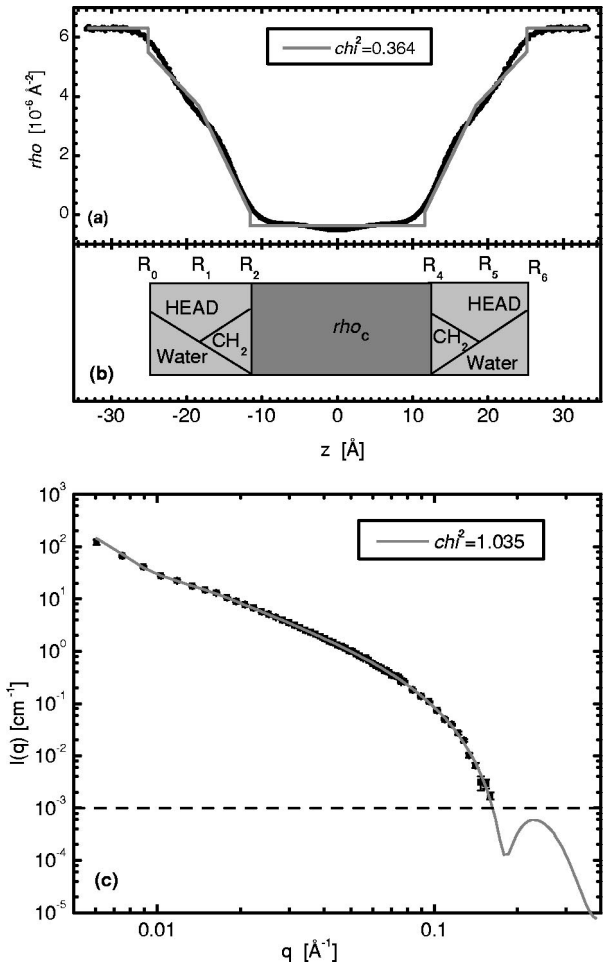

FIG. 7. 3T model: (a) Neutron-scattering length density profile and (b) schematic of the model. See caption to Fig. 3 for description of fitted lines to the MD scattering density profile (a) and scattering curve (c).

Gibbs dividing surface because there is hydrocarbon in the space R_5-R_4. However, the Gibbs dividing surface can be analytically obtained in this linear model from geometric considerations with the result that the thickness of the hydrocarbon region is

$$2D_C = (R_4 - R_2) + (R_6 - R_4)/2 + (N'_W V_W - 2V_H)/4A_L. \quad (9)$$

With these constraints the model again has only two free parameters that may be taken to be D_P (or A_L) and n'_W. The best fit to the scattering data, Fig. 7(c), is as good as in Fig. 4(c) and Fig. 6(c) with completely random residuals (not shown). The resulting scattering density profile is close to the simulated MD profiles as seen in Fig. 7(a). The physical parameters obtained from the fit are shown in Table I.

E. Asymmetrical aspect of vesicles with finite radius

Our presentation has implicitly assumed that the bilayer is symmetric about $z=0$. However, for finite vesicle radius R, Fig. 8 shows that the two monolayers that form the bilayer cannot be symmetrical because the average area per molecule A_6, measured at the vesicular radius where the headgroup resides, must be larger (smaller, respectively) than the area per molecule A_3, measured near the center of the bilayer, when the molecule is in the outer (inner, respectively) monolayer in the vesicle. Indeed, the ratio of these areas must be proportional to the square of the ratio of the radii $(R_6/R_3)^2$. For the outer monolayer, $R_6=300$ Å and $R_3 \approx 275$ Å, so there is a 19% expansion of the molecular area from the center of the bilayer to the end of the headgroup region of the outer monolayer and a similar tapering of the inner monolayer. To develop this picture further and to estimate how much effect this will have on the analysis, there are two constraints that we propose to be applicable to relate the molecular shape of the lipids on the inner and outer monolayers. The first is that the average volume per lipid molecule should be the same in either monolayer. The second is that the headgroup area should be nearly the same for both monolayers at the junction of the hydrocarbon region with the polar regions because the chains are quite flexible and can accommodate the curvature effect more than the headgroups because the latter must satisfy the hydrophobic interfacial interactions with water. With these constraints, the inner monolayer will be thinner than the outer monolayer. Nevertheless, the neutron-scattering length density profile is not much different from the type we have been describing. Since there is no methyl trough where the two monolayers meet, the central hydrocarbon scattering length density remains constant. Only the headgroup regions are perturbed by vesicle curvature. Without loss of generality, we fix the total headgroup volume to be constant and then the curvature effect is quantitated by the relative change in the thickness D_P of the polar region. For vesicles of outer radius $R=300$ Å, curvature increases (decreases) D_P by 3% in the inner (outer, respectively) monolayer compared to a flat bilayer. We have fit data with this feature included and have found that it makes negligible changes. For ease of presentation, we have therefore not included it.

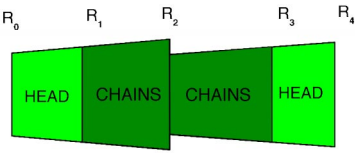

FIG. 8. Sketch of projected lipid volumes in an asymmetrical bilayer due to a radius of curvature which was chosen to be only 200 Å to accentuate the asymmetry.

IV. DISCUSSION

Table I compares the values of the bilayer parameters obtained by fitting our models to the simulated scattering curves. The single-strip model only has one parameter, the width $2D_L$ of the strip. This thickness is clearly a compromise between the hydrocarbon thickness $2D_C$ and the true steric thickness $2D_L$. Nevertheless, the corresponding area A_L is tolerably close to the area used in the simulation. However, the χ^2 of this model, which has only one free parameter, is significantly larger than for our more refined models,

which have two free parameters. Perhaps even more significant, this model predicts much larger scattering for q values greater than 0.2 Å^{-1} than is predicted by the simulation as can be seen by comparing Fig. 2 with Fig. 3. The nonobservance of coherent scattering for $q > 0.2$ Å^{-1} justifies consideration of better models [6,11,36].

The three improved 3S, 3L, and 3T models that we have considered fit the data very well with excellent values of χ^2. This suggests that it is not realistic to consider models with more than two free parameters to interpret neutron scattering from unilamellar vesicles. These models give more realistic values of the steric membrane thickness $2D_L$ than the single-strip 1S model and they provide estimates for the hydrocarbon thickness $2D_C$. Use of this thickness and the hydrocarbon volume V_C in Eq. (7) then gives values of A_L which are only somewhat smaller than the value used in the simulation. This supports the proposition that small-angle neutron scattering can be used to obtain reliable values for bilayer structural quantities [26,27].

It is important to emphasize that the value of V_C was input into the fit from the value that was obtained directly from the simulation. When analyzing real data it is necessary to obtain V_C from other measurements. This has been done by calculating $V_C = V_L - V_H$ where V_L is the accurately measured lipid volume and V_H is the headgroup volume which is measured in the gel phase [1]. We also note that the simulated lipid volume $V_L = 1215.5$ Å^3 was used to obtain the number of waters n'_W in the headgroup region in Table I.

Of the three improved models, the triangular model gives the best values of D_C, D_L, and A_L because the model was designed to mimic the functional form of the simulated scattering length profile better. In particular, this model assumes that there is twice as much water in the polar headgroup region (which includes the carbonyl groups on the hydrocarbon chains) as hydrocarbon methylenes, that the distribution functions are linear and that the hydrocarbon distribution function decays to zero halfway through the polar region. We believe these assumptions provide good approximations that are not likely to be unduly compromised by variations in bilayer area and thickness for fully hydrated phosphatidylcholine headgroups. For bilayers with other headgroups, we suggest that simulations be done to obtain the appropriate assumptions to analyze neutron-scattering data using this kind of model. If such simulations are not performed, then it might be best just to use the three-strip or the 3L models, recognizing that the values for D_L are likely to be different for these two models.

Guinier approximation

It is interesting to compare the approach in this paper to the classical Guinier approximation which obtains the radius of gyration (R_g) from the Kratky-Porod plot [$\ln(Iq^2)$ vs q^2] in the "Guinier region" ($\pi/R < q < 1/R_g$). For a uniform, single-strip model the bilayer thickness is expressed by

$$D_L^2 = 3R_g^2. \tag{10}$$

For our DPPC simulation this gives $D_L = 20.4$ Å, and a rather small $A_L = V_L/D_L = 59.6$ Å^2 as shown by the KP entry in Table II.

TABLE II. Structural parameters using standard (1S) and model Guinier approximation. Asterisk (*) denotes assumed values of parameters.

Model	n'_W	A_L (Å^2)	D_P (Å)	D_C (Å)	D_L (Å)
MD	~11.9	62.9	~10.8	14.2	~25
KP	0*	59.6			20.4
1	0*	62.6			19.4
3S	11.6	62.7	10.8*	14.2	22.5
3L	10.5	59.6	10.8*	15.0	25.8
3T	11.2	61.3	10.8*	14.5	25.3

A recent effort to improve this method first fits experimental data to obtain R_g [25–27]. Then, the parameters in models of the same general type as have been considered in this paper were varied until the same R_g was obtained in the model scattering curve. One advantage of this procedure is that the approximation involved in neglecting the higher order moments (e.g., $\langle R^4 \rangle$) in extracting R_g is the same for the data and for the model. In particular, the value $D_L = 19.4$ Å that is obtained for the 1S model is smaller than for the KP model in the preceding paragraph, and the resulting A_L is satisfyingly close to the actual value used in the simulation as shown in Table II.

In comparison to the model fitting introduced in this paper, the previous method [25–27] could only fit one independent parameter because the amount of experimental information extracted from the data was limited to the Kratky-Porod slope. Therefore, for the results shown for the more realistic models in Table II, another parameter had to be assumed, and the value of the polar headgroup width D_P was arbitrarily fixed to 10.8 Å (or $R_6 - R_4 = 13.6$ Å for triangular model). This arbitrary choice works well for the 3S model, given that D_L has a different interpretation than shown in Fig. 1. However, a different D_P would favor a different model. This indeterminacy is eliminated by the analysis described in Sec. III.

In conclusion, we propose that neutron-scattering data from unilamellar vesicles of lipid bilayers, data that are obtainable outside the Guinier range, be analyzed using models with two independent parameters. The models we have introduced in this paper have been inspired and tested by long molecular dynamics simulations of phosphatidylcholine bilayers; such simulations should continue to inform the construction of future models for analysis of membranes composed of other lipids.

ACKNOWLEDGMENTS

This study was supported by the Slovak Ministry of Education VEGA Grant No. 1/0123/03 to PB, Comenius University Grant No. UK/13/2002 to NK, NSF Grant No. MCB-0091508 to SEF, and by NIH Grant No. GM44976 to JFN.

[1] J. F. Nagle and S. Tristram-Nagle, Biochim. Biophys. Acta **1469**, 159 (2000).
[2] J. Lyatskaya, Y. Liu, S. Tristram-Nagle, J. Katsaras, and J. F. Nagle, Phys. Rev. E **63**, 011907 (2000).
[3] D. Uhríková, N. Kučerka, A. Islamov, V. Gordeliy, and P. Balgavý, Gen. Physiol. Biophys. **20**, 183 (2001).
[4] D. Uhríková, N. Kučerka, A. Islamov, A. Kuklin, V. Gordeliy, and P. Balgavý, Biochim. Biophys. Acta **1611**, 31 (2003).
[5] B. A. Lewis and D. M. Engelman, J. Mol. Biol. **166**, 211 (1983).
[6] J. Pencer and F. R. Hallett, Phys. Rev. E **61**, 3003 (2000).
[7] P. Balgavý, M. Dubničková, D. Uhríková, S. Yaradaikin, M. A. Kiselev, and V. I. Gordeliy, Acta Phys. Slov. **48**, 509 (1998).
[8] V. I. Gordeliy, L. V. Golubchikova, A. Kuklin, A. G. Syrykh, and A. Watts, Prog. Colloid Polym. Sci. **93**, 252 (1993).
[9] W. Knoll, J. Haas, H. B. Stuhrmann, H. H. Füldner, H. Vogel, and E. Sackmann, J. Appl. Crystallogr. **14**, 191 (1981).
[10] S. Komura, Y. Toyoshima, and T. Takeda, Jpn. J. Appl. Phys., Part 1 **21**, 1370 (1982).
[11] P. C. Mason, B. D. Gaulin, R. M. Epand, G. D. Wignall, and J. S. Lin, Phys. Rev. E **59**, 3361 (1999).
[12] T. Nawroth, H. Conrad, and K. Dose, Physica B **156&157**, 477 (1989).
[13] D. Uhríková, P. Balgavý, N. Kučerka, A. Islamov, V. Gordeliy, and A. Kuklin, Biophys. Chem. **88**, 165 (2000).
[14] R. J. Gilbert, R. K. Heenan, P. A. Timmins, N. A. Gingles, T. J. Mitchell, A. J. Rowe, J. Rossjohn, M. W. Parker, P. W. Andrew, and O. Byron, J. Mol. Biol. **293**, 1145 1999).
[15] D. P. Tieleman, S. J. Marrink, and H. J. C. Berendsen, Biochim. Biophys. Acta **1331**, 235 (1997).
[16] D. J. Tobias, K. C. Tu, and M. L. Klein, Curr. Opin. Colloid Interface Sci. **2**, 15 (1997).
[17] R. W. Pastor, Curr. Opin. Struct. Biol. **4**, 486 (1994).
[18] H. Petrache, S. E. Feller, and J. F. Nagle, Biophys. J. **72**, 2237 (1997).
[19] E. Lindhal and O. Edholm, Biophys. J. **79**, 426 (2000).
[20] S. E. Feller, and R. W. Pastor, J. Chem. Phys. **111**, 1281 (1999).
[21] S. W. Chiu, M. Clark, V. Balaji, H. L. Scott, and E. Jakobssen, Biophys. J. **69**, 1230 (1995).
[22] B. R. Brooks, R. E. Bruccoleri, B. D. Olafson, D. J. States, S. Swaminathan, and M. Karplus, J. Comput. Chem. **4**, 187 (1983).
[23] S. E. Feller, and A. D. MacKerell, J. Phys. Chem. **104**, 7510 (2000).
[24] R. S. Armen, O. D. Uitto, and S. E. Feller, Biophys. J. **75**, 734 (1998).
[25] P. Balgavý, N. Kučerka, V. I. Gordeliy, and V. G. Cherezov, Acta Phys. Slov. **51**, 53 (2001).
[26] P. Balgavý, M. Dubničková, N. Kučerka, M. A. Kiselev, S. P. Yaradaikin, and D. Uhríková, Biochim. Biophys. Acta **1512**, 40 (2001).
[27] N. Kučerka, M. A. Kiselev, and P. Balgavý, Eur. Biophys. J. (to be published).
[28] O. Glatter and O. Kratky, *Small Angle X-ray Scattering* (Academic Press, New York, 1982).
[29] L. A. Feigin and D. I. Svergun, *Structure Analysis by Small-Angle X-ray and Neutron Scattering* (Plenum, New York, 1987).
[30] M. A. Kiselev, D. Lombardo, A. M. Kisselev, and P. Lesieur, JINR Dubna Report No. E19-2003-33, 2003 (unpublished).
[31] M. Gradzielski and H. Hoffmann, Adv. Colloid Interface Sci. **42**, 149 (1992).
[32] H. Schmiedel, P. Jörchel, M. Kiselev, and G. Klose, J. Phys. Chem. B **105**, 111 (2002).
[33] Yu. M. Ostanevich, JINR Dubna Report No. P13-87-407, 1987 (unpublished).
[34] V. A. Vagov, A. B. Kunchenko, Yu. M. Ostanevich, and I. M. Salamatin, JINR Dubna Report No. P14-83-898, 1983 (unpublished).
[35] Yu. M. Ostanevich, Makromol. Chem., Macromol. Symp. **15**, 91 (1988).
[36] M. Hirai, H. Iwase, T. Hayakawa, M. Koizumi, and H. Takahashi, Biophys. J. **85**, 1600 (2003).
[37] N. Kučerka, A. Islamov, V. Gordeliy, and P. Balgavý, Proceedings of the XII International Conference on Small-Angle Scattering Venice, Italy, 2002 (unpublished), p. 107.
[38] S. Tristram-Nagle, Y. Liu, J. Legleiter, and J. F. Nagle, Biophys. J. **83**, 3325 (2002).